THE JOURNAL OF PHYSICAL CHEMISTRY Letters

Letter

Cite This: J. Phys. Chem. Lett. 2018, 9, 6841−6846

pubs.acs.org/JPCL

Flexoelectricity in Monolayer Transition Metal Dichalcogenides

Wenhao Shi, Yufeng Guo,* Zhuhua Zhang, and Wanlin Guo

State Key Laboratory of Mechanics and Control of Mechanical Structures and MOE Key Laboratory for Intelligent Nano Materials and Devices, College of Aerospace Engineering, Nanjing University of Aeronautics and Astronautics, Nanjing 210016, China

Supporting Information

ABSTRACT: Flexoelectricity, the coupling effect of the strain gradient and charge polarization, is an important route to tune electronic properties of low-dimensional materials. Here our extensive first-principles calculations reveal that structural wrinkling and corrugation will cause significant flexoelectricity in transition metal dichalcogenide (TMD) monolayers. The flexoelectricity is induced by the strain gradients created along the finite thickness of the wrinkled TMD monolayers and becomes more dominant in determining out-of-plane polarizations with decreasing wavelengths of the TMD wrinkles. According to the first-principles calculations and whole structural symmetry, a theoretical model is developed to describe the total out-of-plane polarizations and flexoelectric effect of the wrinkled TMD monolayers. The unveiled flexoelectricity in monolayer TMDs highlights a potential for their application in energy conversion devices.

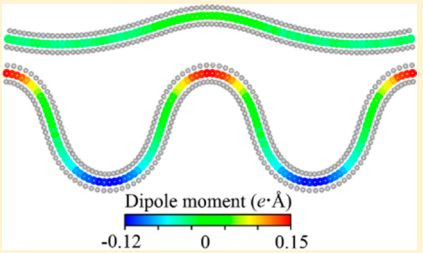

Flexoelectricity, the coupling of electronic and mechanical behaviors that describes electric polarization arising from a mechanical strain gradient or mechanical response under an electric field gradient, has been widely investigated in various types of materials including ferroelectric crystalline materials,[1,2] nematic liquid crystals,[3,4] soft matters, and biomembranes.[5,6] Besides conventional piezoelectricity, the flexoelectric effect provides an alternative method for device applications in sensing,[7] actuating,[8,9] ferroelectric memory,[10] and electricity harvesting.[11,12] To attain noticeable flexoelectricity, macroscale matters and materials usually require large deformation to create strain gradients, which will probably cause structural failure and fracture. On the contrary, small strains on nanoscale materials such as nanotubes, nanowires, and two-dimensional (2D) materials would give rise to large strain gradients. Moreover, 2D materials can also endure large out-of-plane deformation.[13,14] As demands for size miniaturization of functional devices to improve performance and efficiency continue to rise, a need for nanoscale materials becomes essential and urgent. Previous theoretical works have studied flexoelectricity in hexagonal boron nitride (h-BN),[15] graphene nanoribbons,[16] carbon nanoshells,[17] and nanocones,[18] and the corresponding theoretical models have been established to describe the flexoelectricity in carbon materials. However, the flexoelectric effect revealed by those first-principles calculations mainly comes from symmetry breaking of the π orbital charge distribution caused by flexural deformation or curvature, and the induced polarization therefore is weak.[16−18]

Two-dimensional transition metal dichalcogenides (TMDs) are semiconducting and have excellent optoelectronic properties, making them good candidates for photodetection and light-emitting devices.[19−24] In several experiments, 2D MoS_2 materials are found to possess strong in-plane piezoelectricity and piezotronic effects, which could be used in piezoelectric and triboelectric nanogenerators.[25−28] Recently, another experiment reports that monolayer MoS_2 exhibits remarkable out-of-plane polarization when a compressive loading exerted by the tip of atomic force microscopy acts on it, and the enhancement of vertical piezoelectricity in the MoS_2 is explained by the possible flexoelectric effect induced by structural deformation.[29] However, the underlying mechanism to produce flexoelectricity in TMDs still remains elusive. Most of the former theoretical modeling of flexoelectricity for 2D materials focuses on hBN and carbon nanostructures of one atomic layer, and no further model is developed for TMD nanostructures. With one or a few atom-layer thickness, 2D materials can easily undergo out-of-plane deformation. As a consequence, wrinkles and ripples are commonly observed for graphene, h-BN, and TMDs when they are under compressive constraint or substrate influence. Structural corrugation of 2D materials not only changes their intrinsic properties but also endows them with new physical phenomena and application potential. For example, wrinkle-induced local strain can tune the direct band gap and photogenerated excitons of atomically thin MoS_2.[30] Now it is also technically feasible to fabricate periodic wrinkled nanostructures with controllable geometries.[11,31] On the other hand, the wrinkling of 2D materials leads to nonuniform deformation, which could cause a significant strain gradient. Further understanding the influence of structural wrinkling and corrugation on the charge polarization in monolayer TMDs will be of importance in unveiling their flexoelectricity.

In this study, we reveal by first-principles calculations that structural wrinkling and corrugation in TMD monolayers give rise to significant flexoelectricity. With increasing wrinkling deformation, the flexoelectric effect gradually becomes the key

Received: October 31, 2018
Accepted: November 18, 2018
Published: November 19, 2018

DOI: 10.1021/acs.jpclett.8b03325
J. Phys. Chem. Lett. 2018, 9, 6841−6846

role in determining charge polarization at each atom. The combining and synergistic effects of strain gradient-dependent flexoelectricity and structural symmetry dominate the total polarizations of the wrinkled TMD monolayers. On the basis of the dipole moments and compressive forces calculated from density function theory (DFT), we develop a theoretical model to describe the total out-of-plane polarizations and flexoelectricity in the TMD monolayers.

We first consider a flat 2H $MoSe_2$ monolayer that has 62 Mo and 124 Se atoms in a rectangle unit cell with a length of 102.84 Å in the x direction and a width of 5.75 Å in the y direction. The wrinkled geometry or structure is created by gradually reducing the length of the unit cell to apply uniaxial compression on the $MoSe_2$ monolayer and simultaneously rearranging the positions of each atoms. The state-of-the-art DFT technique is employed to obtain a stable wrinkled structure and calculate the total or global z-direction dipole moment D_z^t with respect to the center mass of the wrinkle. Then the vertical polarization P_z of the $MoSe_2$ wrinkle is estimated by $P_z = D_z^t/A$, where A is the area of the initial flat $MoSe_2$ monolayer.

The stable wrinkled $MoSe_2$ with different wavelengths W are shown in Figure 1. With decreasing wavelength, the curvatures

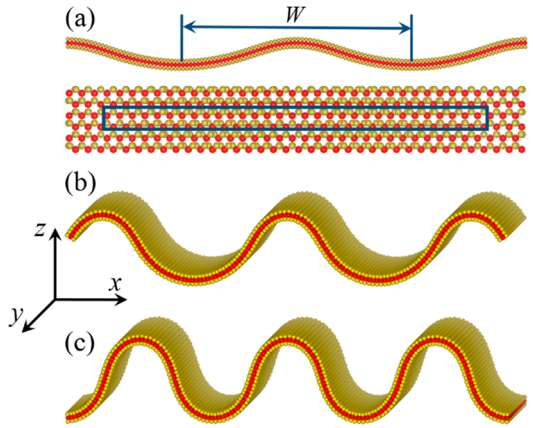

Figure 1. Relaxed structures of the wrinkled $MoSe_2$ monolayers with wavelengths of (a) 9.8 nm, side and top views, (b) 8.0, and (c) 6.6 nm. In (a), the blue rectangle represents the unit cell, and W is the wavelength after wrinkling, which is the same as the length of the unit cell. The periodic boundary conditions are applied in the x and y directions, and the red and yellow dots are Mo and Se atoms, respectively.

and bending deformation at the wrinkle top and bottom increase. Table 1 presents the calculated compression force F_x, vertical polarization P_z, dipole moment D_z^t, and energy gap E_g, which are the global values of the wrinkled $MoSe_2$ monolayers. The compression force to hold the wrinkled geometry obviously decreases after the wrinkle transforms into a state

Table 1. Longitudinal Compression Force F_x, Vertical Polarization P_z, Dipole Moment D_z^t, and Energy Gap E_g of the Wrinkled $MoSe_2$ with Different Wavelengths

	9.8 nm	8.0 nm	6.6 nm
F_x (nN)	1.83	0.55	0.51
P_z (pC/m)	−0.005	0.182	0.152
D_z^t (e·Å)	−0.002	0.067	0.056
E_g (eV)	1.5	1.273	1.29

with a smaller wavelength, which can be ascribed to buckling-induced bond relaxation.[32] For the flat $MoSe_2$ monolayer, the vertical or out-of-plane polarization is approximately zero. In a small wrinkle or slight rippling such as the wrinkle with a wavelength of 9.8 nm, the vertical polarization is also very low. Only if the wrinkle is large enough, the vertical polarization becomes significant. It should be pointed out that the polarization does not monotonically increase with the wavelength decreases, as shown in Table 1. The same as the flat state, the wrinkled $MoSe_2$ monolayer is still semiconducting, but the structural corrugation and deformation reduce the energy gap.

In the $MoSe_2$ monolayer, there are three atomic layers along the thickness, and the flexural wrinkling will give rise to nonuniform bond changes. The Mo atoms locate at the middle layer; thus, the bending deformation causes compression and tension on the two Se layers. Accordingly, strain gradients are inevitably created along the thickness direction of the $MoSe_2$ layer. Each Mo atom connects with six Se atoms in the $MoSe_2$ monolayer, where three Se atoms are above the Mo atom and another three below. The flexural deformation leads to different length changes in the Se−Mo bonds (see Figure S1 in the Supporting Information). As the $MoSe_2$ monolayer only has three atomic layers, it is difficult to give an accurate thickness. In our study, the strain gradient at each Mo atom of the wrinkled $MoSe_2$ along its finite thickness is approximately defined by $\Delta\varepsilon = \Delta\varepsilon'/t$; here $\Delta\varepsilon' = (l^b_{Se-Mo} - l^t_{Se-Mo})/l_{Se-Mo}$, t is the thickness of the monolayer, l_{Se-Mo} is the initial Se−Mo bond length at the flat state, and l^t_{Se-Mo} and l^b_{Se-Mo} are the average lengths of the three Se−Mo bonds where the Se atoms are above and below the Mo atoms, respectively. The z-direction dipole moment of the Mo atom is estimated by $D_{Mo} = \int \rho(r) r \, d^3r$, where $\rho(r)$ is the charge density in the range of the Wigner−Seitz radius around the Mo atom and r is the distance to the atomic center. Figure 2a shows the variations of the dipole moments of the Mo atoms with strain gradients. For

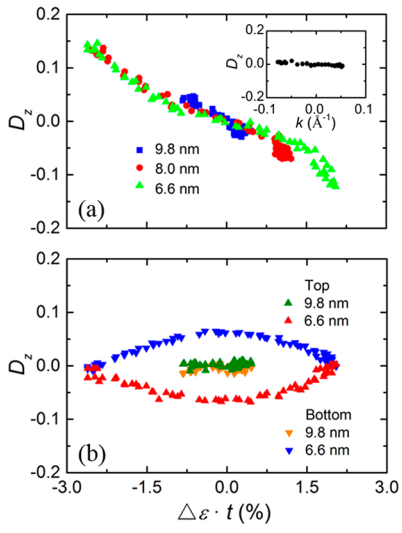

Figure 2. Dipole moments (in units of e·Å) of (a) the Mo atoms with strain gradients for wavelengths of 9.8 (square), 8.0 (circle), and 6.6 nm (triangle) (the inset shows the dipole moments of the C atoms in the wrinkled graphene monolayer with a wavelength of 6.6 nm). (b) Se atoms for wavelengths of 9.8 and 6.6 nm. Here the up and down triangles represent the Se atoms above and below the Mo atoms, respectively.

DOI: 10.1021/acs.jpclett.8b03325
J. Phys. Chem. Lett. 2018, 9, 6841−6846

the wrinkled monolayer of W = 9.8 nm, the dipole moments of the Mo atoms are small because of the weak flexural deformation. The maximum dipole moments and strain gradients increase with the wavelength decreases. All of the variations of the z-direction dipole moments are approximately linear with the strain gradients, and the variation slopes of the three cases are approximately identical, demonstrating the validity of the definition of the atomic strain gradient. Those results indicate that the flexoelectric effect gradually becomes dominant as the changes in the Mo−Se bonds and Mo−Mo distances of the wrinkled monolayer are nonuniform and the magnitude of wrinkling deformation increases (see Figure S1 in the Supporting Information). For comparison, we have also studied the polarization of the wrinkled graphene monolayer by the same method and procedure. The inset in Figure 2a shows the dipole moments of the C atoms with its curvature k for the wrinkled graphene with a wavelength of 6.6 nm. Here the curvature k of each C atom in the wrinkled graphene monolayer is estimated by $k = \frac{|Z''|}{[1+(Z')^2]^{3/2}}$, where Z is the fitting function of the z-direction displacements of the C atoms, and Z' and Z'' are the first and second derivatives of Z with respect to the x coordinates, respectively. Obviously, the polarizations at the C atoms are much weaker than those at the Mo atoms, which is consistent with previous studies.[16−18] Therefore, the flexoelectric effect induced in the TMD monolayer is much stronger than that in graphene and hBN. Moreover, the dipole moments of the Se atoms are given in Figure 2b. It is clearly shown that the z-direction dipole moments of the Se atoms above and below the Mo atoms are symmetric with the zero dipole moment, and thus, the dipole moments of the top Se atoms will cancel out with that of the bottom Se atoms when considering the global polarization of the wrinkle.

To better describe the flexoelectricity induced in the wrinkled $MoSe_2$ monolayers, Figure 3 shows the contour plots of the dipole moments of the Mo atoms. The polarizations at the top and bottom parts of the wrinkles are enhanced with the wavelength decreases. It can also be seen from Figures 2 and 3 that the difference between the negative and positive dipole moments decreases with improving structural symmetry of the wrinkle. Charges move to the compressive sites of the wrinkled monolayer, and higher curvature leads to stronger charge polarization; see Figure S2 in the Supporting Information. Nevertheless, the polarization direction at the wrinkle top is obviously opposite to that at the wrinkle bottom. The total z-direction polarization of the wrinkled $MoSe_2$ is therefore weakened by the cancellation effect from the wrinkle top and bottom parts, which is directly related to its structural symmetry.

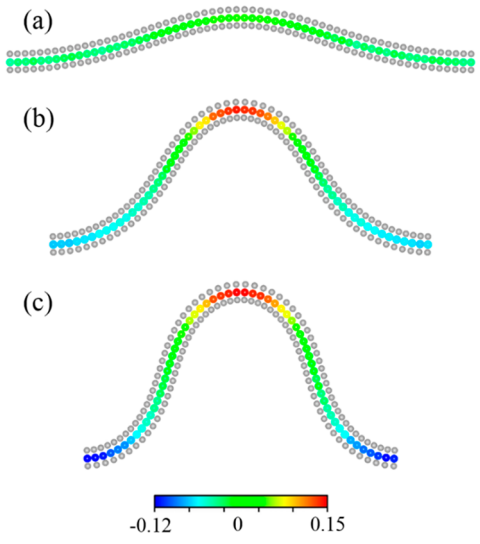

Figure 3. Contour plots of the atomic dipole moments of the Mo atoms (in units of e·Å) for the wrinkled $MoSe_2$ monolayers with wavelengths of (a) 9.8, (b) 8.0, and (c) 6.6 nm.

The conventional model to describe polarizations P_i^* that involve both piezoelectric and flexoelectric effects[33−35] is usually expressed by

$$P_i^* = P_{\text{piez}}^* + P_{\text{flex}}^* = d_{ijk}\sigma_{jk} + f_{ijkl}\frac{\partial \varepsilon_{jk}}{\partial x_l} \tag{1}$$

where σ_{jk} are stresses, d_{ijk} are third-rank piezoelectric tensors, $\frac{\partial \varepsilon_{jk}}{\partial x_l}$ are strain gradients, and f_{ijkl} represent the components of flexoelectric tensors. Regarding the wrinkled $MoSe_2$ monolayer, only the z-direction polarization is considered; therefore, eq 1 for the wrinkling polarization becomes

$$P_z^* = d_{zx}\sigma_x + f_{zx}\frac{\partial \varepsilon_x}{\partial z} \tag{2}$$

In eq 2, $P_z^* = \frac{D_z^t}{At}$, and the strain gradient $\frac{\partial \varepsilon_x}{\partial z}$ of the wrinkle is actually difficult to compute. According to the symmetries of the bond length changes in the Mo−Se bonds and the dipole moments of the Mo atoms (shown in Figures S1 and 2), the $\frac{\partial \varepsilon_x}{\partial z}$ is approximately estimated by $\frac{\partial \varepsilon_x}{\partial z} = \frac{S_2 - \mu S_1}{S_1 t}$, where μ is a proportion parameter and S_2 and S_1 are the projected areas of top and bottoms parts of the wrinkle with respect to the position of the z-direction mass center, respectively, as shown by the inset in Figure 4a. We use the item $\frac{\partial \varepsilon_x}{\partial z} = \frac{S_2 - \mu S_1}{S_1 t}$, the difference between the areas above and below the z-direction mass center, to describe the characteristic of structural deformation of the whole wrinkle that includes the entire contributions from all atoms, which can be approximately considered as the average or global influence of strain gradients on the wrinkled $MoSe_2$. Let $\sigma_x = \frac{F_x}{wt}$, $n = \frac{S_2}{S_1}$, where w is the width of the wrinkle and is the same as the unit cell width. Then the formula describing the wrinkling polarization can be derived as

$$P_z^* = \frac{d_{zx}}{wt}F_x + \frac{f_{zx}}{t}(n - \mu) \tag{3}$$

In terms of $P_z = D_z^t/A$ and $P_z^* = \frac{D_z^t}{At}$, eq 3 becomes

$$P_z = P_{\text{piez}}^z + P_{\text{flex}}^z = \frac{d_{zx}}{w}F_x + f_{zx}(n - \mu) \tag{4}$$

In our DFT calculations, we study several TMD wrinkles with different wavelengths. The F_x is the force obtained from the DFT calculation, and other parameters d_{zx}, f_{zx}, and μ in eq 4 are determined by fitting the DFT results of all considered TMD wrinkles and are given in Table 2. Figure 4a shows the comparison between the polarizations of the wrinkled $MoSe_2$ obtained from the modeling of eq 4 and DFT calculations. The deduced polarizations of eq 4 are consistent with those from

DOI: 10.1021/acs.jpclett.8b03325
J. Phys. Chem. Lett. 2018, 9, 6841−6846

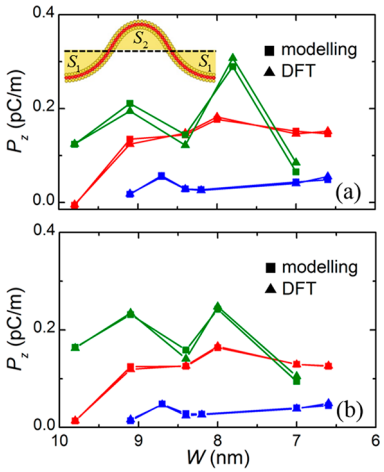

Figure 4. Total z-direction polarizations of the wrinkled TMD monolayers derived by theoretical modeling and DFT calculations with their wavelengths. (a) $MoSe_2$ (red), MoS_2 (blue), and $MoTe_2$ (green) monolayers. The inset shows the defined areas of S_1 and S_2 of the wrinkled monolayer. Here the horizontal dashed line crossing the mass center of the wrinkle separates the projected area into two parts, S_1 and S_2. (b) WSe_2 (red), WS_2 (blue), and WTe_2 (green) monolayers. The square and triangle lines are the results of theoretical modeling and DFT calculations.

the DFT calculations, proving the validity of the theoretical modeling by defining the areas of S_1 and S_2 of the $MoSe_2$ wrinkles. If the wrinkle has a better structural symmetry, the item $f_{zx}(n - \mu)$ will be smaller and the total z-direction polarization will thus be decreased. On the other hand, the piezoelectricity defined by the item $\frac{d_{zx}}{w}F_x$ will impose influence on the total z-direction polarization. Therefore, the final polarization of the wrinkle is determined by the combining effect of strain gradient-dependent flexoelectricity, wrinkle structural symmetry, and compressive stress-induced piezoelectricity.

Additionally, the flexoelectricity in other types of TMD MX_2 (M = Mo or W; X = S, Se, or Te) monolayers has been studied by the same computational procedure and theoretical modeling. The polarizations from the DFT calculations and modeling derivations for the wrinkled MX_2 and the corresponding fitting parameters are presented in Figure 4 and Table 2, respectively. Similar to the wrinkled $MoSe_2$, the total polarizations in other wrinkled TMDs vary with their wavelengths. In the six considered TMD monolayers, the strongest polarization is found to be induced on the $MoTe_2$. All of the polarizations deduced by eq 4 coincide well with the results of the DFT calculations. This consistency further demonstrates the validity and applicability of our theoretical modeling for describing the total polarization of the wrinkled TMD monolayers. Our theoretical model describing the z-direction polarizations P_z of the TMD wrinkles consists of two parts: one is from the piezoelectricity P^z_{piez}, and another is from the flexoelectricity P^z_{flex}. The contributions of piezoelectricity and flexoelectricity to total out-of-plane polarization have been compared for all wrinkled monolayers (see Figure S3 in the Supporting Information). It is clearly shown that the contributions of P^z_{flex} are much larger than those of P^z_{piez} for all wrinkled TMDs; therefore, the flexoelectric effect and structural symmetry play a dominant role in affecting the total polarizations of the wrinkled TMD monolayers. As a result, the out-of-plane polarizations of the TMDs can be effectively tuned by modifying the wrinkling wavelength and structural geometry.

In summary, our extensive first-principles calculations unveil the significant flexoelectricity in TMD monolayers, which is much stronger than that in other 2D materials such as graphene and hBN. A theoretical model is established to describe the total out-of-plane polarizations and flexoelectric effect, and the predictions from the model are consistent with the results of the DFT calculations. The strain gradient-dependent flexoelectricity and structural symmetry dominate the total polarizations of the wrinkled TMDs. Our results provide an attractive way to develop nanoscale energy conversion and sensing devices by utilizing the wrinkling of 2D TMD materials.

COMPUTATIONAL METHODS

All DFT computations were implemented in the VASP code by using the projector augmented wave method with the Perdew–Burke–Ernzerhof (PBE) exchange–correlation functional.[36–38] In the DFT calculations, the periodic boundary conditions were applied in the x and y directions to retain compression and simulate the wrinkles with infinite widths in the y direction, and there is a vacuum region larger than 30 Å in the direction perpendicular to the wrinkle top. All of those systems were relaxed by using a conjugate-gradient algorithm until the force on each atom was less than 0.01 eV/Å. After structural relaxation, an energy cutoff of 500 eV and special k points sampled on a $1 \times 10 \times 1$ γ mesh were used to calculate the z-direction global dipole moment D^t_z with respect to the center mass of the wrinkle.

ASSOCIATED CONTENT

Supporting Information

The Supporting Information is available free of charge on the ACS Publications website at DOI: 10.1021/acs.jpclett.8b03325.

Bond changes and 2D projections of charge densities for the $MoSe_2$ monolayers and absolute values of the ratios of P^z_{flex}/P^z_{piez} for wrinkled TMDs (PDF)

AUTHOR INFORMATION

Corresponding Author

*E-mail: yfguo@nuaa.edu.cn. Tel: +86 25 84890513. Fax: +86 25 84895827.

ORCID

Yufeng Guo: 0000-0002-8378-7288

Table 2. Parameters in the Theoretical Modelling for the Six Wrinkled TMDs

	MoS_2	WS_2	$MoSe_2$	WSe_2	$MoTe_2$	WTe_2
d_{zx} (pm/V)	−0.017	−0.004	−0.055	−0.036	0.009	0.011
f_{zx} (pC/m)	−1.82	−1.60	−0.69	−0.76	−2.26	−2.00
μ	1	1	1.23	1.16	1	1

DOI: 10.1021/acs.jpclett.8b03325
J. Phys. Chem. Lett. 2018, 9, 6841–6846

Zhuhua Zhang: 0000-0001-6406-0959

Notes

The authors declare no competing financial interest.

■ ACKNOWLEDGMENTS

This work is supported by the NSFC (11472131, 51535005, 11622218), the Program for New Century Excellent Talents in University (NCET-13-0855), the NSF of Jiangsu Province (BK20160037), the Fundamental Research Funds for the Central Universities (NJ20150048, INMD-2015M02) of China, and the Research Fund of the State Key Laboratory of Mechanics and Control of Mechanical Structures (Nanjing University of Aeronautics and Astronautics) (MCMS0414G01, 0416K01), a Project Funded by the Priority Academic Program Development of Jiangsu Higher Education Institutions.

■ REFERENCES

(1) Ma, W.; Cross, L. E. Flexoelectricity of Barium Titanate. *Appl. Phys. Lett.* **2006**, *88*, 232902.
(2) Lu, H.; Bark, C. W.; Esque de los Ojos, D.; Alcala, J.; Eom, C. B.; Catalan, G.; Gruverman, A. Mechanical Writing of Ferroelectric Polarization. *Science* **2012**, *336*, 59−61.
(3) Takahashi, T.; Hashidate, S.; Nishijou, H.; Usui, M.; Kimura, M.; Akahane, T. Novel Measurement Method for Flexoelectric Coefficients of Nematic Liquid Crystals. *Jpn. J. Appl. Phys.* **1998**, *37*, 1865.
(4) Harden, J.; Mbanga, B.; Éber, N.; Fodor-Csorba, K.; Sprunt, S.; Gleeson, J. T.; Jakli, A. Giant Flexoelectricity of Bent-Core Nematic Liquid Crystals. *Phys. Rev. Lett.* **2006**, *97*, 157802.
(5) Petrov, A. G.; Ramsey, R. L.; Usherwood, P. N. R. Curvature-Electric Effects in Artificial and Natural Membranes Studied Using Patch-Clamp Techniques. *Eur. Biophys. J.* **1989**, *17*, 13−17.
(6) Porenta, T.; Ravnik, M.; Zumer, S. Effect of Flexoelectricity and Order Electricity on Defect Cores in Nematic Droplets. *Soft Matter* **2011**, *7*, 132−136.
(7) Majdoub, M. S.; Sharma, P.; Cagin, T. Enhanced Size-Dependent Piezoelectricity and Elasticity in Nanostructures Due to the Flexoelectric Effect. *Phys. Rev. B: Condens. Matter Mater. Phys.* **2008**, *77*, 125424.
(8) Shen, Z.; Chen, W. Converse Flexoelectric Effect in Comb Electrode Piezoelectric Microbeam. *Phys. Lett. A* **2012**, *376*, 1661−1663.
(9) Fu, J. Y.; Zhu, W.; Li, N.; Cross, L. E. Experimental Studies of the Converse Flexoelectric Effect Induced by Inhomogeneous Electric Field in a Barium Strontium Titanate Composition. *J. Appl. Phys.* **2006**, *100*, 024112.
(10) Catalan, G.; Noheda, B.; McAneney, J.; Sinnamon, L.; Gregg, J. M. Strain Gradients in Epitaxial Ferroelectrics. *Phys. Rev. B: Condens. Matter Mater. Phys.* **2005**, *72*, 020102.
(11) Qi, Y.; Jafferis, N. T.; Lyons, K., Jr.; Lee, C. M.; Ahmad, H.; McAlpine, M. C. Piezoelectric Ribbons Printed onto Rubber for Flexible Energy Conversion. *Nano Lett.* **2010**, *10*, 524−528.
(12) Wang, Z.; Zhang, X.; Wang, X.; Yue, W.; Li, J.; Miao, J.; Zhu, W. Giant Flexoelectric Polarization in a Micromachined Ferroelectric Diaphragm. *Adv. Funct. Mater.* **2013**, *23*, 124−132.
(13) Zhao, J.; Deng, Q.; Ly, T. H.; Han, G. H.; Sandeep, G.; Rümmeli, M. H. Two-Dimensional Membrane as Elastic Shell with Proof on the Folds Revealed by Three-Dimensional Atomic Mapping. *Nat. Commun.* **2015**, *6*, 8935.
(14) Zhu, W.; Low, T.; Perebeinos, V.; Bol, A. A.; Zhu, Y.; Yan, H.; Tersoff, J.; Avouris, P. Structure and Electronic Transport in Graphene Wrinkles. *Nano Lett.* **2012**, *12*, 3431−3436.
(15) Duerloo, K. A. N.; Reed, E. J. Flexural Electromechanical Coupling: a Nanoscale Emergent Property of Boron Nitride Bilayers. *Nano Lett.* **2013**, *13*, 1681−1686.
(16) Kalinin, S. V.; Meunier, V. Electronic Flexoelectricity in Low-Dimensional Systems. *Phys. Rev. B: Condens. Matter Mater. Phys.* **2008**, *77*, 033403.
(17) Dumitrică, T.; Landis, C. M.; Yakobson, B. I. Curvature-Induced Polarization in Carbon Nanoshells. *Chem. Phys. Lett.* **2002**, *360*, 182−188.
(18) Kvashnin, A. G.; Sorokin, P. B.; Yakobson, B. I. Flexoelectricity in Carbon Nanostructures: Nanotubes, Fullerenes, and Nanocones. *J. Phys. Chem. Lett.* **2015**, *6*, 2740−2744.
(19) Mak, K. F.; Shan, J. Photonics and Optoelectronics of 2D Semiconductor Transition Metal Dichalcogenides. *Nat. Photonics* **2016**, *10*, 216.
(20) Wang, Q. H.; Kalantar-Zadeh, K.; Kis, A.; Coleman, J. N.; Strano, M. S. Electronics and Optoelectronics of Two-Dimensional Transition Metal Dichalcogenides. *Nat. Nanotechnol.* **2012**, *7*, 699.
(21) Jariwala, D.; Sangwan, V. K.; Lauhon, L. J.; Marks, T.; Hersam, M. C. Emerging Device Applications for Semiconducting Two-Dimensional Transition Metal Dichalcogenides. *ACS Nano* **2014**, *8*, 1102−1120.
(22) Lopez-Sanchez, O.; Lembke, D.; Kayci, M.; Radenovic, A.; Kis, A. Ultrasensitive Photodetectors Based on Monolayer MoS2. *Nat. Nanotechnol.* **2013**, *8*, 497.
(23) Rivera, P.; Schaibley, J. R.; Jones, A. M.; Ross, J. S.; Wu, S.; Aivazian, G.; Klement, P.; Seyler, K.; Clark, G.; Ghimire, N. J.; et al. Observation of Long-Lived Interlayer Excitons in Monolayer $MoSe_2$-WSe_2 Heterostructures. *Nat. Commun.* **2015**, *6*, 6242.
(24) Ross, J. S.; Klement, P.; Jones, A. M.; Ghimire, N. J.; Yan, J.; Mandrus, D. G.; Taniguchi, T.; Watanabe, K.; Kitamura, K.; Yao, W.; et al. Electrically Tunable Excitonic Light-Emitting Diodes Based on Monolayer WSe_2 P-N Junctions. *Nat. Nanotechnol.* **2014**, *9*, 268−272.
(25) Duerloo, K. A. N.; Ong, M. T.; Reed, E. J. Intrinsic Piezoelectricity in Two-Dimensional Materials. *J. Phys. Chem. Lett.* **2012**, *3*, 2871−2876.
(26) Wu, W.; Wang, L.; Li, Y.; Zhang, F.; Lin, L.; Niu, S.; et al. Piezoelectricity of Single-Atomic-Layer MoS_2 for Energy Conversion and Piezotronics. *Nature* **2014**, *514*, 470.
(27) Wu, C.; Kim, T. W.; Park, J. H.; An, H.; Shao, J.; Chen, X.; Wang, Z. L. Enhanced Triboelectric Nanogenerators Based on MoS_2 Monolayer Nanocomposites Acting as Electron-Acceptor Layers. *ACS Nano* **2017**, *11*, 8356−8363.
(28) Liu, J.; Goswami, A.; Jiang, K.; Khan, F.; Kim, S.; McGee, R.; Li, Z.; Hu, Z.; Lee, J.; Thundat, T. Direct-Current Triboelectricity Generation by a Sliding Schottky Nanocontact on MoS_2 Multilayers. *Nat. Nanotechnol.* **2018**, *13*, 112−116.
(29) Brennan, C. J.; Ghosh, R.; Koul, K.; Banerjee, S. K.; Lu, N.; Yu, E. T. Out-of-Plane Electromechanical Response of Monolayer Molybdenum Disulfide Measured by Piezoresponse Force Microscopy. *Nano Lett.* **2017**, *17*, 5464−5471.
(30) Castellanos-Gomez, A.; Roldán, R.; Cappelluti, E.; Buscema, M.; Guinea; van der Zant, F. H. S.; Steele, G. A. Local Strain Engineering in Atomically Thin MoS_2. *Nano Lett.* **2013**, *13*, 5361−5366.
(31) Wang, Y.; Yang, R.; Shi, Z.; Zhang, L.; Shi, D.; Wang, E.; Zhang, G. Super-Elastic Graphene Ripples for Flexible Strain Sensors. *ACS Nano* **2011**, *5*, 3645−3650.
(32) Guo, Y.; Qiu, J.; Guo, W. Tunable Bending Stiffness of $MoSe_2$/WSe_2 Heterobilayers from Flexural Wrinkling. *Nanotechnology* **2017**, *28*, 195701.
(33) Kogan, S. M. Piezoelectric Effect during Inhomogeneous Deformation and Acoustic Scattering of Carriers in Crystals. *Sov. Phys. Solid State.* **1964**, *5*, 2069−2070.
(34) Jiang, X.; Huang, W.; Zhang, S. Flexoelectric Nano-Generator: Materials, Structures and Devices. *Nano Energy* **2013**, *2*, 1079−1092.
(35) Deng, Q.; Liu, L.; Sharma, P. Flexoelectricity in Soft Materials and Biological Membranes. *J. Mech. Phys. Solids* **2014**, *62*, 209−227.
(36) Kresse, G.; Furthmüller, J. Efficient Iterative Schemes for Ab Initio Total-Energy Calculations Using a Plane-Wave Basis Set. *Phys. Rev. B: Condens. Matter Mater. Phys.* **1996**, *54*, 11169.

DOI: 10.1021/acs.jpclett.8b03325
J. Phys. Chem. Lett. 2018, 9, 6841−6846

(37) Blöchl, P. E. Projector Augmented-Wave Method. *Phys. Rev. B: Condens. Matter Mater. Phys.* **1994**, *50*, 17953.
(38) Perdew, J. P.; Burke, K.; Ernzerhof, M. Generalized Gradient Approximation Made Simple. *Phys. Rev. Lett.* **1996**, *77*, 3865.

DOI: 10.1021/acs.jpclett.8b03325
J. Phys. Chem. Lett. 2018, 9, 6841−6846